Electron Holography on Beam Sensitive Materials: Organic Polymers and Mesoporous Silica

Paul Simon,*,† Ralf Huhle,† Michael Lehmann,† Hannes Lichte,† Damian Mönter,‡ Thomas Bieber,‡ Wladimir Reschetilowski,‡ Rameshwar Adhikari,§ and Goerg H. Michler§

Institute of Applied Physics, University of Dresden, Zellescher Weg 16, D-01062 Dresden, Germany, Institute of Technical Chemistry, University of Dresden, Mommsenstrasse 4, D-01062 Dresden, Germany, and Institute of Materials Science, University of Halle-Wittenberg, Geusaer Strasse, D-06217 Merseburg, Germany

Received May 28, 2001. Revised Manuscript Received November 20, 2001

For the investigation of weak phase objects such as polymers by means of conventional electron microscopy, the objects have to be stained prior to imaging or imaged under strong defocus to find a sufficient contrast in the image. However, these techniques bear the risk of artifacts, e.g., chemical staining and the appearance of Fresnel diffraction phenomena occurring during defocus. These artifacts do not appear with holography. Therefore, holograms of ultrathin sections (50−70 nm) of organic block copolymer were recorded, and the corresponding phase images were reconstructed. In this way, typical structures such as lamellae and onion patterns could be imaged without any staining. In addition, we successfully recorded holograms of mesoporous silica molecular sieve MCM-41 which show the hexagonal arrangement of uniformly sized porosities without using defocus. Holography has been demonstrated as a feasible tool to image beam sensitive and weak phase objects without artifacts.

1. Introduction

Up to date, imaging of weak phase objects still poses a severe challenge to conventional electron microscopy. For organic objects, besides the low contrast, beam sensitivity causes the main restriction to imaging techniques. Organic polymers, for example, show explicit sensitivity to beam damage as a consequence of inelastic interactions. Therefore, the resolution is finally controlled by the critical dose. Already, in the very beginning of electron microscopy, several methods were developed to overcome these difficulties. Chemical staining and defocus are the most commonly used techniques for weak phase objects. Recently, low-voltage microscopy has shown promising results despite the requirement of very thin samples.[1]

Electron holography[2−5] is mainly used in materials science to image ceramic structures and metals and their alloys. For example, in semiconductor research, holography is used to image the interface between doped layers, the so-called p−n junctions.[6−8] Ceramics are interesting because of their superconductivity, ferroelectricity, and giant magnetoresistance (GMR).[9,10] For biological science or polymer research, holography is not a common technique yet. This may be due to the explicit beam sensitivity of the proteins and DNA on one hand. On the other hand, biologists and polymer scientists often know only quite little about electron holography. Nevertheless, some attempts have been made to image polymeric and biological samples by holography.[11−16]

In general, the electron wave leaving the object ("object exit wave") is modulated by elastic interaction in amplitude a and phase φ as

$$o(x) = a(x) \times \exp(i\varphi(x))$$

For weak phase objects, the assumptions $a(x) \approx 1$ and $\varphi(x) = C_E V_p$ hold with the "projected potential" $V_p := \int$

* To whom correspondence should be addressed. Tel: 49-351-4633-3579. Fax: 49-351-4633-3199. E-mail: Simon@physik.tu-dresden.de.
† Institute of Applied Physics, University of Dresden.
‡ Institute of Technical Chemistry, University of Dresden.
§ University of Halle-Wittenberg.

(1) Coufalova, E.; Delong, A. *Proc. EUREM 12*, Brno, Czech Republic **2000**, *1*, 183.
(2) Lichte, H. *Adv. Opt. Electron. Microsc.*; Mulvay, T., Sheppard, T. R., Eds.; Academic Press: New York, 1991; Vol. 12, p 25.
(3) Van Dyck, D. *J. Electron Microsc.* **1999**, *48*, 33.
(4) Lehmann, M.; Lichte, H.; Geiger, D.; Lang, G.; Schweda, E. *Mater. Charact.* **1999**, *42*, 249.
(5) Midgley, P. A. *Micron* **2000**, *32*, 167.
(6) Frabboni, S.; Matteucci, G.; Pozzi, G.; Vanci, M. *Phys. Rev. Lett.* **1985**, *55* (20), 2196.
(7) Rau, W. D.; Schwander, P.; Ourmazd, A. *Solid State Phenom.* **1998**, *63−64*, 525.
(8) McCartney, M. R.; Ponce, F. A.; Cai, J.; Bour, D. P. *Appl. Phys. Lett.* **2000**, *76* (21), 3055.
(9) Ravikumar, V.; Rodrigues, R. P.; Dravid, V. P. *J. Am. Ceram. Soc.* **1997**, *80* (5), 1117.
(10) Johnson, K. D.; Dravid, V. P. *Appl. Phys. Lett.* **1999**, *74* (4), 621.
(11) Kawasaki, T.; Endo, J.; Matsuda, T.; Osakabe, N.; Tonomura, A. *J. Electron Microsc.* **1986**, *35*, 211.
(12) Aoyama, K.; Ru, Q. *J. Microsc.* **1996**, *182*, 177.
(13) Wang, Y. C.; Chou, T. M.; Libera, M.; Voelkl, E.; Frost, B. G. *Microsc. Microanal.* **1998**, *4*, 146.
(14) Dunin-Borkowski, R. E.; McCartney, M. R.; Frankel, R. B.; Bazylinski, D. A.; Posfai M.; Buseck, P. R. *Sci. Int. Ed. AAAS* **1998**, *282*, 1868.
(15) Weierstall, U. Diploma Thesis, University of Tübingen, Germany, 1989.
(16) Harscher, A. Ph.D. Thesis, University of Tübingen, Germany, 1999.

10.1021/cm011140q CCC: $22.00
Published on Web 03/20/2002

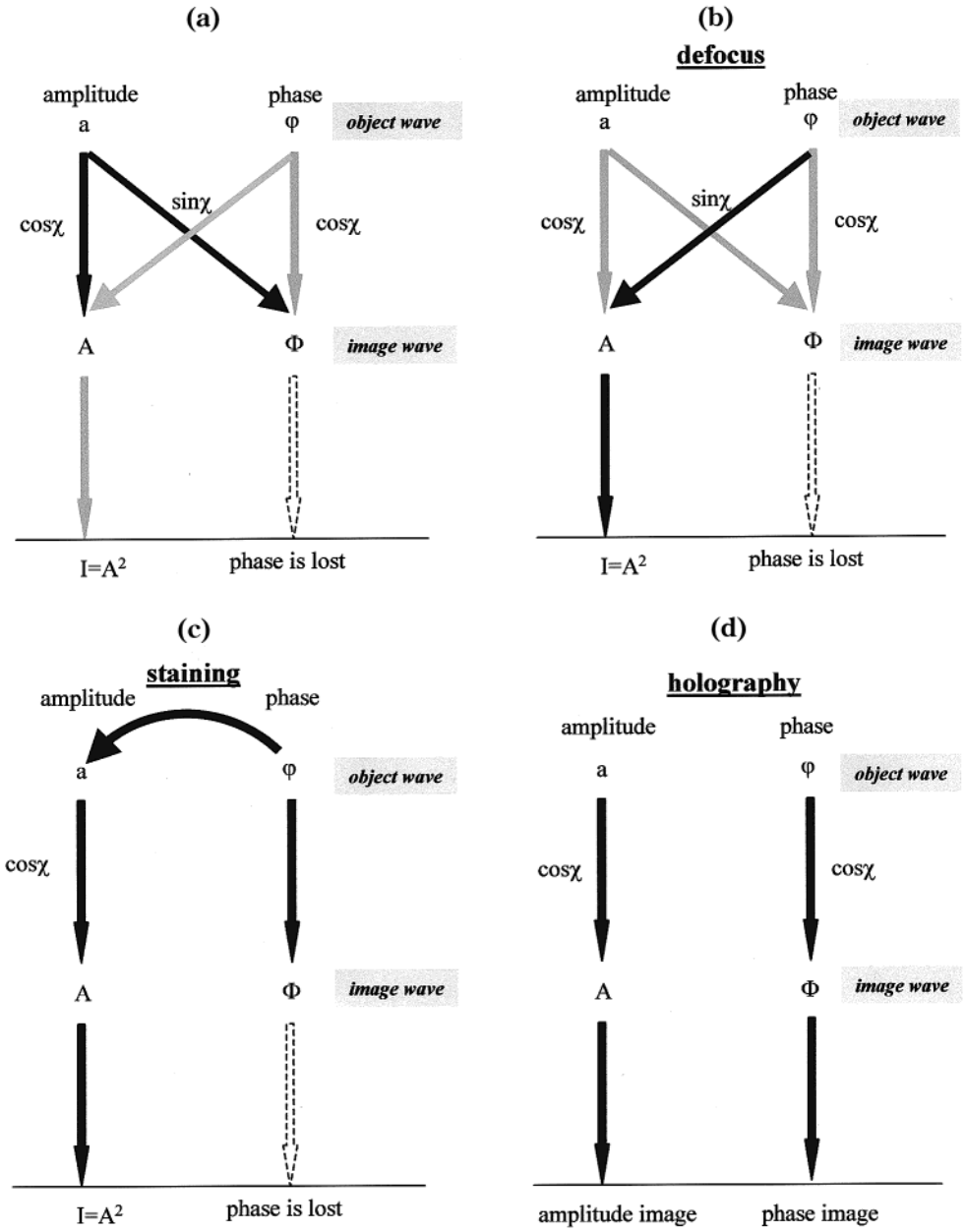

Figure 1. (a) Information flux in the electron microscope. The phase φ of the object is transformed into the amplitude A of the image by the PCTF $= -\sin\chi$. The amplitude a of the object is directly transferred by the ACTF $= \cos\chi$ into the amplitude A of the image. Correspondingly, the object amplitude is transferred into amplitude and phase of the image wave. (b) Defocus technique makes use of conventional phase contrast: the phase φ of the object is transferred to the amplitude A of the image by PCTF $= -\sin\chi$. (c) Image formation for stained samples: the object phase φ is transformed to an object amplitude a by heavy metal adsorption. (d) Image formation for holography: phase and amplitude of the object are transferred to the image wave and are recorded simultaneously.

$V(x,y,z)$ dz integrated along the electron path through the object. C_E is the interaction constant of the particular microscope.

The transfer of the wave in the electron microscope is best described by means of Fourier optics according to Abbe theory of microscopy. In the Fourier plane, i.e., the diffraction pattern of the object wave, the "wave transfer function" (WTF)

$$\mathrm{WTF}(q) = B(q) \times \exp(i\chi(q))$$

dampens the spatial frequencies q by the aperture $B(q)$ and induces a phase shift according to the so-called wave aberration

$$\chi(q) = 2\pi k(0.25C_s(q/k)^4 + 0.5D_z(q/k)^2)$$

where $k = 1/\lambda$ is the reciprocal electron wavelength, C_s is the coefficient of spherical aberration of the objective lens, and D_z is the defocus selected by the operator. Schematically, the flux of information through the optical system is sketched in Figure 1a: the image wave

$$b(x) = A(x) \times \exp(i\Phi(x))$$

found on the final screen is the result of the combined action of the phase contrast transfer function (PCTF)

$$\mathrm{PCTF}(q) = -\sin(\chi(q))$$

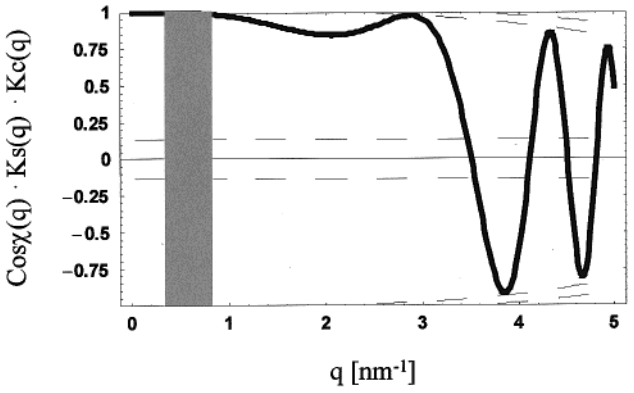

Figure 2. In electron holography, the phase transfer function cosχ (full line) corresponding to the amplitude contrast-transfer function (ACTF) cosχ is used at Gabor focus $\Delta f = -38$ nm. The chromatic (K_c) and illumination (K_s) envelope functions (dotted line) are damping transfer due to energy width and restricted lateral coherence of illumination. Spatial frequency of large area object is indicated.

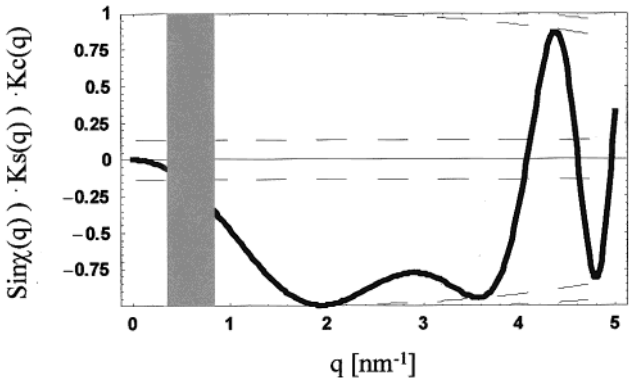

Figure 3. In conventional electron microscopy, the phase contrast transfer function sinχ is used at Scherzer focus $\Delta f = -68$ nm.

and the amplitude contrast-transfer function (ACTF)

$$\mathrm{ACTF}(q) = \cos(\chi(q))$$

on amplitude a and phase φ of the object exit wave. Examples of ACTF and PCTF are shown in Figures 2 and 3.

In conventional electron microscopy, the image intensity $I(x) = b(x)b'(x) = A^2(x)$ is recorded whereas the image phase $\Phi(x)$ is lost (Figure 4). Therefore, by means of a suitable defocus, the object phase $\varphi(x)$ has to be directed into the image amplitude $A(x)$ to be recordable at a sufficient contrast given by the PCTF. Usually, Scherzer focus (Figure 3) is selected to transfer the maximum possible bandwidth of spatial frequencies. Scherzer focus is given by

$$D_z = -1.2(C_s\lambda)^{1/2}$$

where λ is the electron wavelength. If the structures of interest are larger than the atomic details (e.g., polymers), one has to apply a much stronger underfocus to visualize them with a sufficient contrast. This, however, produces artifacts like delocalization and further causes deterioration of resolution.

In conventional electron microscopy, the structures of weak phase objects are visualized either by chemical staining or defocus. Beside these techniques, there exist additional methods for contrast enhancement like strain-induced contrast enhancement or irradiation with γ-rays.[17] In the following section, we discuss the imaging and contrast formation using these conventional techniques and compare them with electron holography.

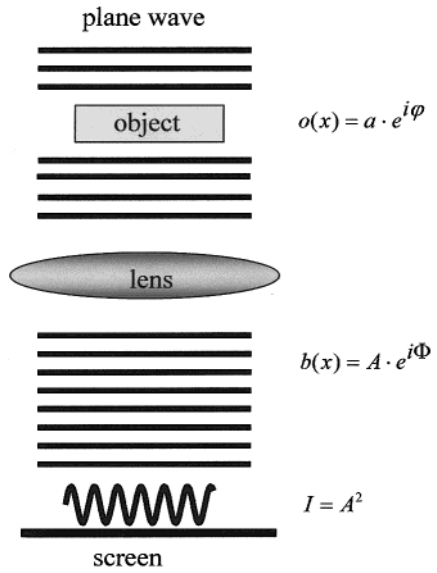

Figure 4. Conventional electron microscopy: phase information Φ is lost in the micrograph.

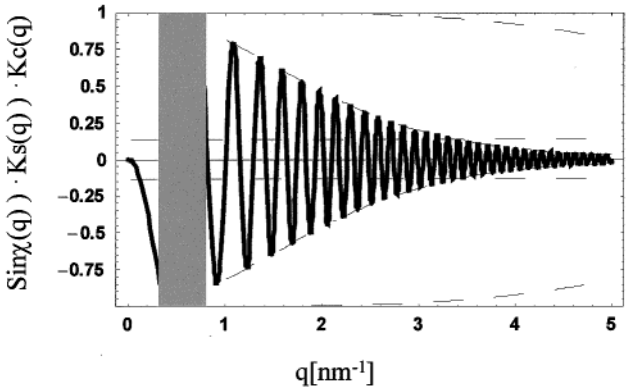

Figure 5. Phase contrast transfer function sinχ for strong defocus $\Delta f = -1.2$ μm.

Defocus. With the use of the defocus technique, the transfer of the object phase into the amplitude of the image according to the PCTF $= -\sin\chi$ can be optimized (Figure 1b). Large area objects display poor contrast at small defocus values such as at Scherzer focus (Figure 3). Hence, we have to defocus strongly to image large area objects.[18] If we defocus strongly, the spacings of interest (marked with the hatched region in Figure 5) are transferred with a sufficient contrast, but the oscillations of the PCTF cause a remarkable loss of resolution for finer spacing (Figure 5). At strong underfocus, the appearance of Fresnel fringes at the edges of the sample make the image interpretation quite difficult. The defocus technique was first applied by Petermann et al.[19] for polymers, and later on, it proved to be successful for block copolymers as well.[20]

(17) Michler, G. H. *Appl. Spectrosc. Rev.* **1993**, *28*, 327.
(18) Reimer, L. *Transmission Electron Microscopy*; Springer publisher: 1989.
(19) Petermann, J.; Gleiter, H. *J. Polym. Sci., Part B: Polym. Phys. Ed.* **1975**, *13*, 1939.

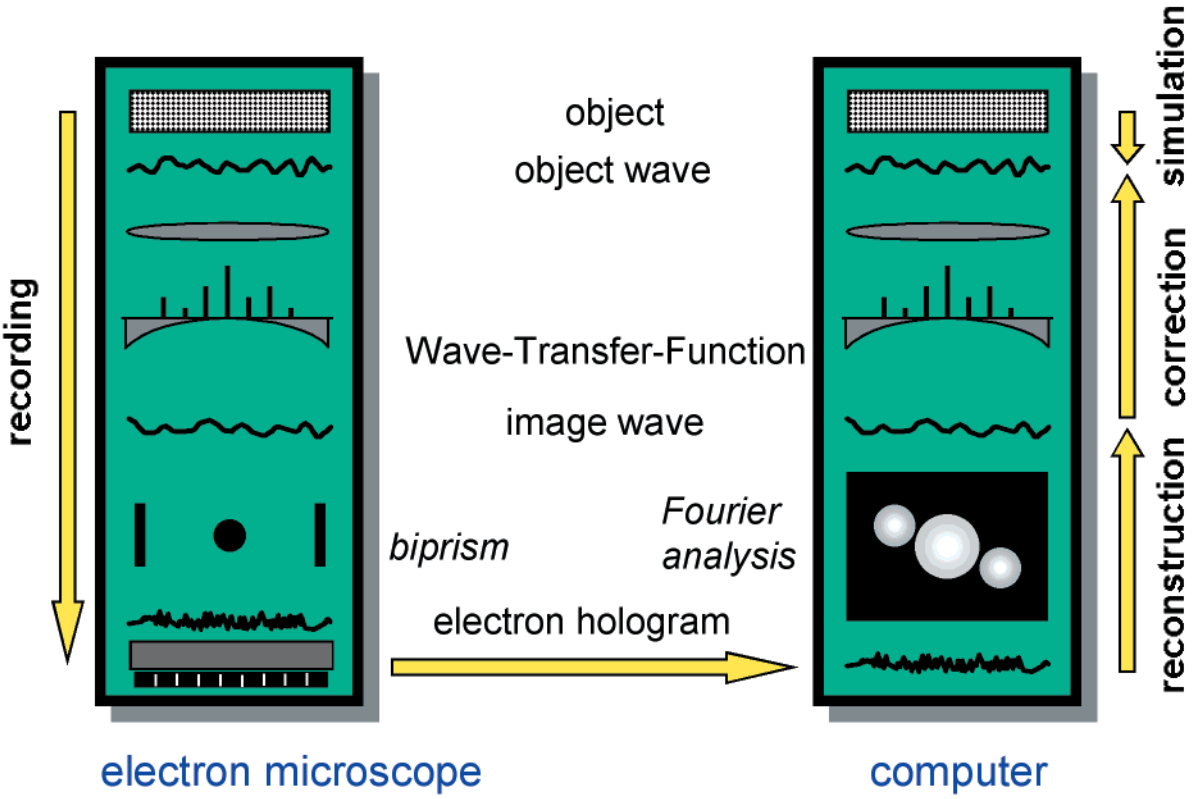

Figure 6. Recording and reconstruction of electron holograms.

Staining. In particular, for small spatial frequencies, smaller than, e.g., 1 nm^{-1}, corresponding to spacings of larger than 1 nm, the ACTF would be much superior. Therefore, often by staining, the object phase structures are converted into an object amplitude structure hence transferred along the path governed by the ACTF. Then, alas, artifacts may arise from selective deposition caused by specific chemical reactions as well as coalescence and grain formation of the staining.

Staining with heavy metal compounds is an established method to achieve contrast of large area weak phase objects.[21] These compounds react with polymers in a highly selective manner. The heavy metal compound penetrates certain regions of the sample and produces strong contrast by scattering absorption. In this way, the weak phase object is transferred into an amplitude object (Figure 1c). Subsequently, the amplitude of the object wave will be converted into the image wave by the amplitude contrast-transfer function (ACTF; see Figure 2).

Staining offers some advantages in comparison with defocus. First, the structure of the sample is less sensitive to radiation damage. Thus, beam damage will not play that role, and furthermore, one obtains a very good contrast. However, there are some severe disadvantages: the selectivity of the staining compound can be poor, pronouncing wrong details. Additionally, the grain size of the heavy metal restricts the upper limit of resolution for the structure of interest. For example, the grain size of osmium tetroxide amounts to 10−15 Å.

(20) Hendlin, D. L., Jr.; Thomas, E. L. *Macromolecules* **1983**, *16*, 1514.
(21) Bremer, A.; Henn, C.; Engel, A.; Baumeister, W.; Aebi, U. *Ultramicroscopy* **1992,** *46*, 85.

Holography. The difficulties of imaging weak phase objects by means of conventional electron microscopy give rise to the question of whether it is possible to achieve better results by electron holography. In holography, both phase and amplitude of the image wave, transferred simultaneously (Figure 1d) as given by the amplitude and phase transfer functions, are recorded as follows (Figure 6): The illuminating wave is divided into two parts, i.e., the object and reference wave. The object wave propagates through the object and is modulated in amplitude and phase according to the object structure. The reference wave goes through vacuum and hence is not affected by the object. An electron biprism superimposes reference and object waves in the image plane, giving rise to an interference pattern,

$$I_{\mathrm{hol}}(x) = 1 + A^2(x) + 2A(x)\cos[2\pi q_c x + \Phi(x)]$$

the so-called hologram (Figure 7), where q_c is the spatial frequency of the interference fringes. The biprism consists of a positively charged wire arranged between the objective lens and the first intermediate image. To achieve a high contrast of the hologram fringes, a monochromatic and coherent illumination as provided by a field emission gun (FEG) is indispensable.

After magnification by means of the subsequent lenses, the hologram is recorded by a CCD camera. The digitized image is transferred to a computer where amplitude and phase of the recorded wave can be reconstructed separately by means of numerical image processing. For this, the Fourier transform of the hologram

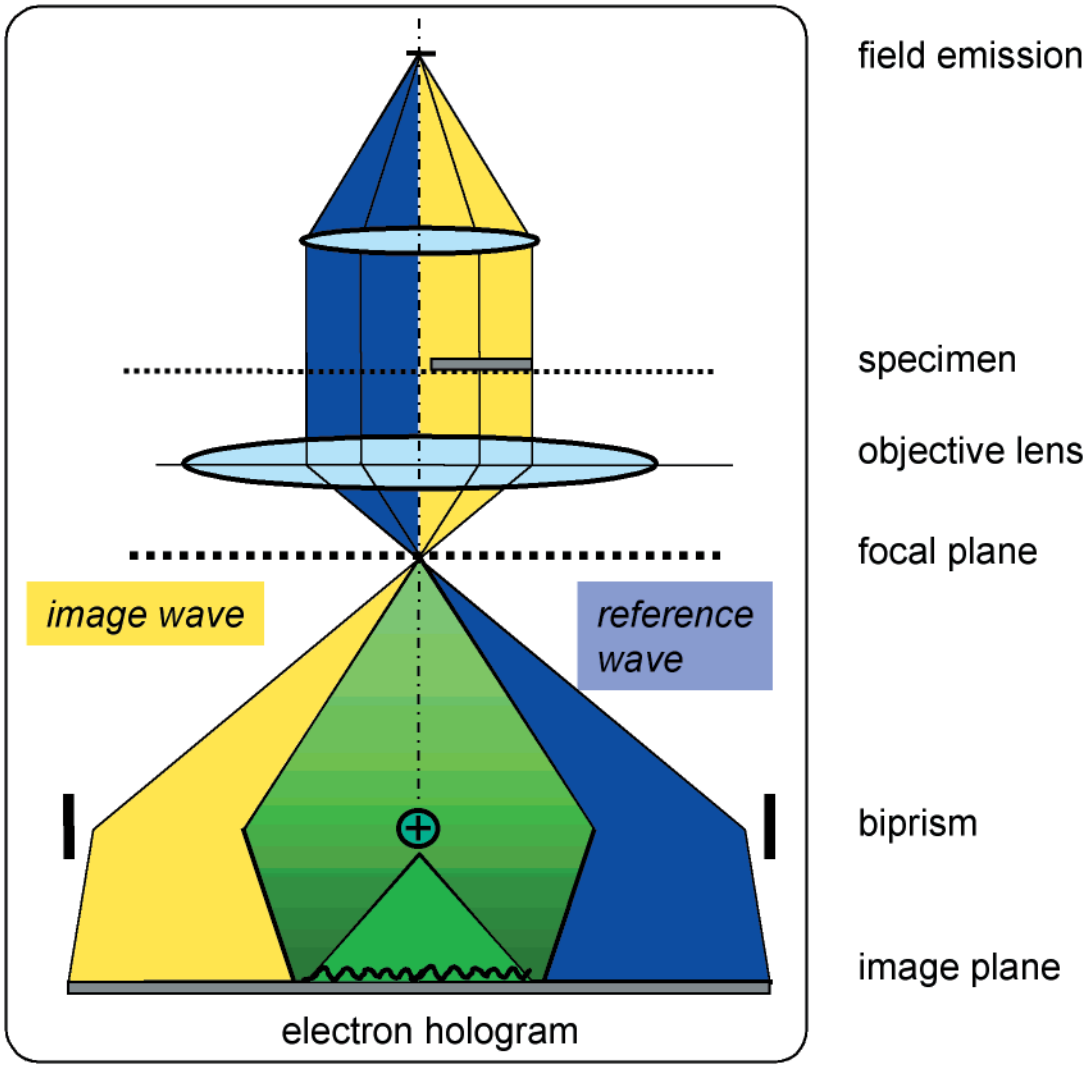

Figure 7. Off-axis electron holography set up.

$$\mathrm{FT}[I_{\mathrm{hol}}] = \delta(q) + \mathrm{FT}[A] \quad \text{centerband}$$
$$+ \delta(q - q_c) \otimes \mathrm{FT}[A \times \exp(i\Phi)] \quad \text{sideband } +1$$
$$+ \delta(q + q_c) \otimes FT[A \times \exp(-i\Phi)] \quad \text{sideband } -1$$

is determined. One obtains three bands: the centerband corresponds to the diffractogram of the common intensity distribution only, whereas each of the sidebands contains the Fourier spectrum of the complete wave. It is sufficient to use one of the (redundant) sidebands to reconstruct phase Φ and amplitude A. Usually, the sideband +1 is masked out and centered to the origin of Fourier space; after inverse Fourier transform, both amplitude image and phase image of the image wave

$$b(x) = A(x) \times \exp(i\Phi(x))$$

are reconstructed in real space. Consequently, as sketched above, these images are still affected by the transfer functions of the objective lens. In Fourier space, it is possible to correct for the aberrations of the objective lens and thus improve resolution. For the applications discussed here, however, this is not needed because, by using Gabor focus under hologram recording, one obtains an excellent transfer for large area objects down to very low spatial frequencies (Figure 2).[22] The hatched region represents the spatial frequencies of interest. Gabor focus is given by $D_{z\ \mathrm{Gabor}} = 0.56 D_{z\ \mathrm{Scherzer}}$. Evidently, with holography, defocus and staining are not needed. The big advantage of holography is the detection of very small phase shifts in the sample without any treatment of the sample (e.g., staining) or the microscope parameters (e.g., defocus or low voltage). As a disadvantage, it should be mentioned that, in comparison with conventional electron microscopy, the essential irradiation dose is higher by a factor 2.

Effect of Inelastic Scattering. The weak interaction of the electrons with atoms of low atomic number provides poor contrast. Therefore, larger thickness of the samples is required. The thicker the sample, the more is the accumulated phase shift

$$\varphi = C_{\mathrm{E}} \times V_{\mathrm{p}} = C_{\mathrm{E}} \times \bar{U} \times d$$

where $\bar{U}$ is the mean inner potential and d is sample thickness (Figure 8).

However, with increasing thickness, inelastic scattering also grows. Inelastically scattered electrons are not coherent with the reference wave and thus destroy

(22) Lichte, H. *Ultramicroscopy* **1991**, *38*, 13.

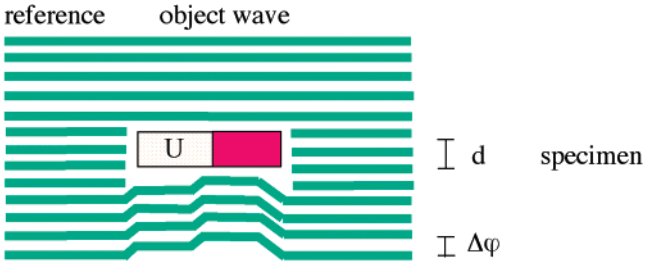

Figure 8. Phase shift $\Delta\varphi$ is depending on thickness d and inner potential $\bar{U}$ of the specimen.

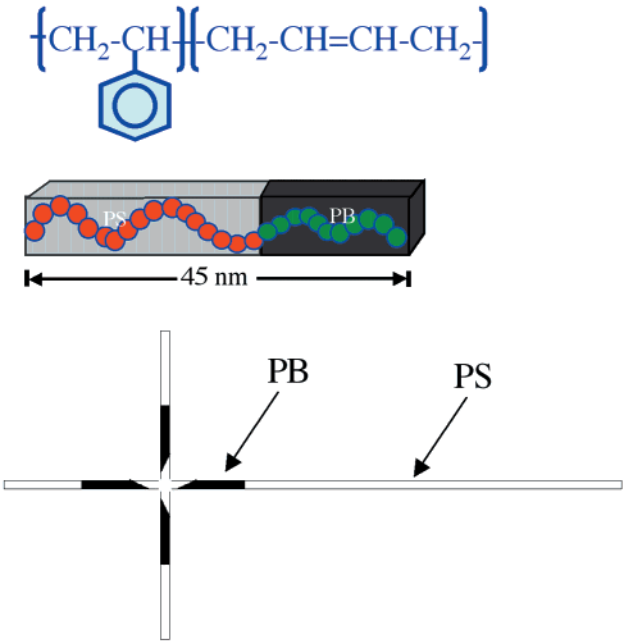

Figure 9. Organic star block copolymer composed of styrene and butadiene segments. The periodicity of the lamellae as measured in the reconstructed electron phase image of the copolymer (Figure 14) amounts to 45 nm.

contrast by producing noisy underground of the signal. Consequently, to maximize the signal/noise ratio of the recorded wave, one has to optimize the sample thickness, producing a measurable phase shift and simultaneously minimizing inelastic scattering.

2. Experimental Section

2.1. Materials. Organic star block copolymer and mesoporous silica MCM-41 material were investigated. Both are weak phase objects and, in addition, they show explicit beam sensitivity.

2.1.1. Block Copolymer. As the polymer, we have chosen a lamellar star block copolymer consisting of styrene and butadiene block chains (molecular fraction of polystyrene $\phi_{PS} = 0.74$, molecular weight $M_n = 103\,000$ g/mol). Styrene/butadiene block copolymers represent microphase-separated systems having highly ordered structures (like spheres, cylinders, lamellae, etc.) whose periodicity lies in the range of radius of gyration R_g of copolymer molecules. Since the dimension of phase-separated structures is well below the wavelength of visible light, the products are transparent and hence find applications as packaging films. Through the variation of composition, mechanical properties of the block copolymers can be tailored.

The copolymer used in this study has a highly asymmetric structure with respect to the length of the polystyrene (PS) end blocks.[23] The PS and polybutadiene (PB) block chains self-assemble to form alternating PS and PB lamellae as illustrated schematically in Figure 9.

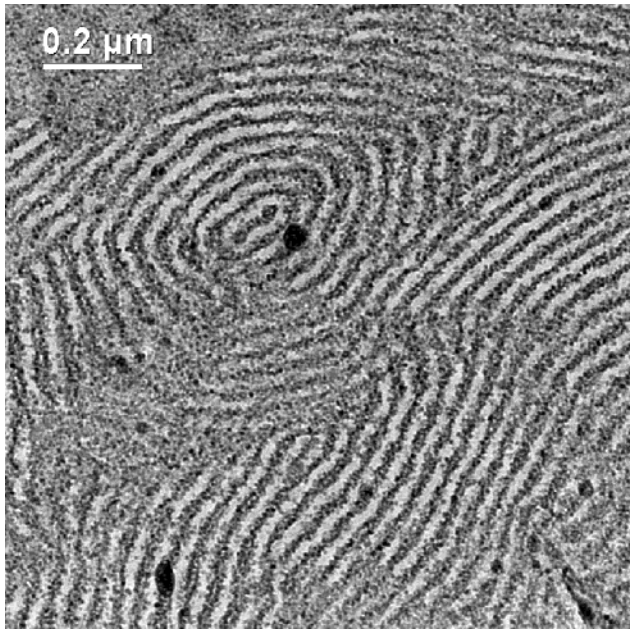

Figure 10. Conventional electron micrograph of stained thin section of styrene/butadiene block copolymer.

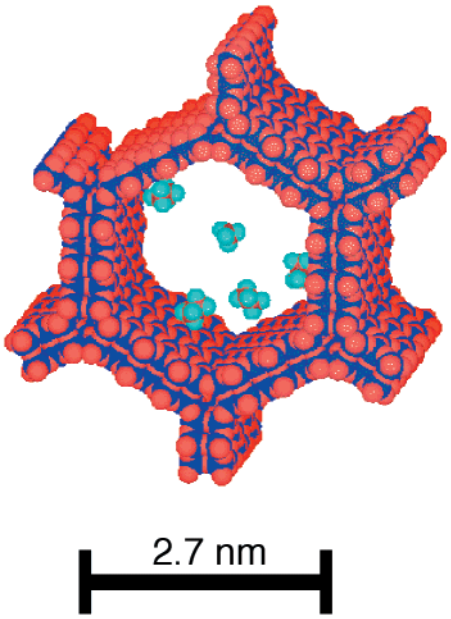

Figure 11. Hexagonally shaped unit cell of mesoporous silica MCM − 41 with small alkane molecules.

Sample Preparation. Thin films of bulk materials were obtained by thin sectioning. Since the films showed high absorption and charging effects at thickness of 100 nm and more, ultrathin sections of the samples with a thickness in the range of 50−70 nm were prepared using an ultramicrotome (Leica, Ultracut UCT equipped with cooling chamber FCS operated at −120 °C) with a diamond knife (Diatome company) for the holographic investigations. The thin sections were spread on Cu grids without support film. The film size amounted to about 0.2 × 0.2 mm^2. The holograms were taken at the edges of the specimen, since the holographic reference beam must run through vacuum next to the sample. The top of the thin section was covered with a thin carbon film with a thickness of about 5 nm to avoid charging of the specimen.

(23) Knoll, K.; Niessner, N. *Macromol. Symp.* **1998**, *132*, 231.

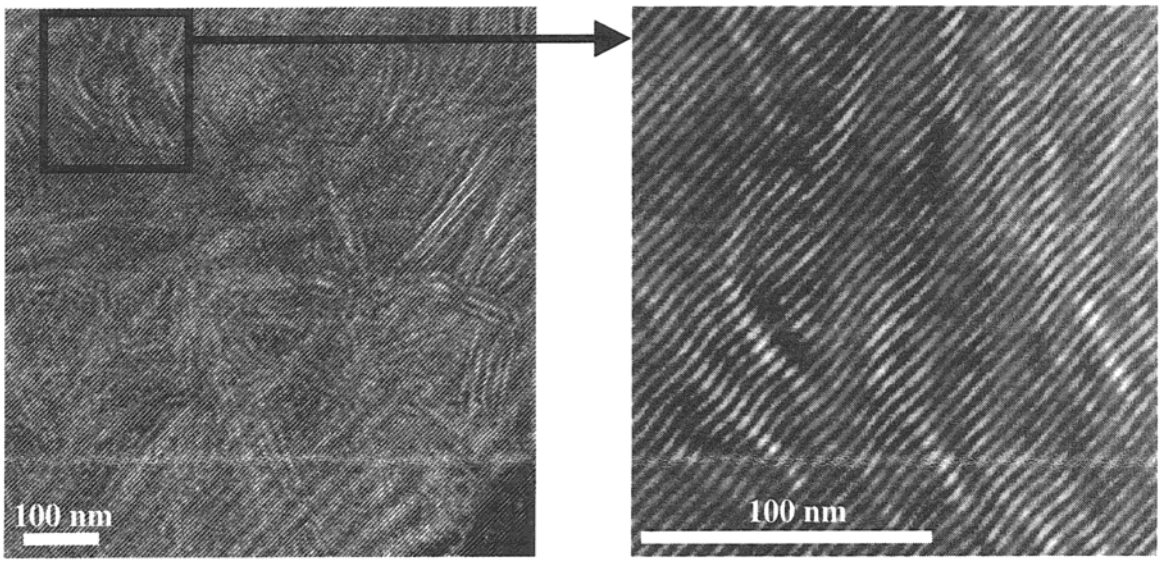

Figure 12. (a) Electron hologram of stained polyethylene crystalline lamellae and (b) zoomed image with distorted hologram fringes indicating strong phase shift.

For comparison with conventional electron microscopy, a small block of sample was dipped into aqueous osmium tetroxide (OsO_4) solution for several hours to selectively stain the butadiene phase according to the method of Kato,[24] so that the polybutadiene phase appears dark in TEM images (see Figure 10). Subsequently, ultrathin sections (ca. 70 nm) were ultramicrotomed at room temperature.

2.1.2. Mesoporous Silica. As a second sample, we have chosen an inorganic mesoporous silica, designated as MCM-41 (Mobil's Composition of Matter, structure 41). This molecular sieve belongs to the M41S family, from which materials have been first synthesized in 1992 by the Mobil Co.[25] The large surface area (>900 m^2/g) and the pore size in the range of 1.5−10 nm, depending on the synthesis procedure, makes them particularly interesting for applications in industrial processes as catalysts or catalyst supports.[26−28] By incorporation of heteroatoms such as titanium, zirconium, or vanadium, the so-called redox molecular sieves can be prepared, which are active catalysts for the liquid-phase oxidation of organic molecules with large kinetic diameters.[29]

Synthesis of the Mesoporous Silica MCM-41. The silica MCM-41 material was synthesized according to a slightly modified procedure published by Franke et al.[30] Dodecyltrimethylammonium bromide ($C_{12}H_{25}(CH_3)_3N^+Br^-$, DTMABr) was used as template. The molar gel composition was SiO_2: 0.195, (tetraethylammoniumhydroxide) TEAOH:0.286, DTMABr:31, and H_2O. After hydrothermal treatment for 24 h, the solid was recovered by filtration and washed with 1.5 L of bidistilled water. The solid was then dried in air at 120 °C for 12 h and eventually calcined with the following temperature program: 1.1 °C/min to 120 °C, 1 h at 120 °C in N_2, 1.1 °C/min to 540 °C, 1 h at 540 °C in N_2, and finally 11.8 h at 540 °C in air.

The powder was characterized by X-ray diffraction by means of a Philips D 5000 diffractometer using the Cu Kα radiation. It gives a highly resolved XRD pattern, which can be indexed on a hexagonal lattice with a calculated unit cell parameter a_0 = 3.52 nm (d_{100} = 3.05 nm, $a_0 = 2d_{100}/3^{1/2}$). A BET (Brunauer−Emmett−Teller isotherm) surface area of 1100 m^2/g was determined from the N_2 adsorption−desorption isotherms. These data were collected at 77 K on a sorptomatic 1900 (Carlo Erba) volumetric sorption equipment designed for measuring specific surfaces, pore volumes, and diameters.

Before the TEM investigations, the resulting powder was suspended in ethanol by ultrasonic treatment. The suspension was brought onto a Cu grid coated with a holey carbon foil. The dispensable liquid was removed by filter paper.

The material consists of a hexagonal arrangement of channels with uniformly sized pores. The walls of the channels are composed of amorphous silica (SiO_2), which forms a continuous polymer network. In Figure 11, a unit cell of a hexagonal lattice is shown with alkane molecules.[31] For an electron microscope, these silicates are weak phase objects and the porosities become visible only at strong defocus.[32]

2.2. Electron Microscopy and Holography. The specimens were investigated by means of a Philips CM200 FEG\ST Lorentz electron microscope equipped with a FEG operated at the acceleration voltage of 200 kV. The silicate was examined in normal mode of the objective lens. At a magnification of 554000×, the hologram fringe spacing, related to the object, amounts to 0.16 nm at a biprism voltage of 190 V. For the investigation of the polymer, the Lorentz mode was found much more favorable. It yields a larger field of view of about 600 × 600 nm at a magnification of 40500×. The applied biprism voltage of about 160 V results in a hologram fringe spacing of about 4.05 nm. Special precautions against beam damage (like use of low-dose technique or cooling stage) were not yet taken. Micrographs and holograms are recorded with a 1k*k CCD camera and fed to a computer for on-line image processing and reconstruction nearly in real time.

In addition to each hologram of a specimen, an "empty hologram" without any object was recorded for subsequent correction of the geometric distortion of the fringes stemming from the projection lenses and the CCD camera; without this

(24) Kato, K. *J. Electron Microsc.* **1965**, *14*, 220.
(25) Beck, J. S.; Vartuli, J. C.; Roth, W. J.; Leonowicz, M. E.; Kresge, C. T.; Schmitt, K. D.; Chu, C. T. W.; Olson, D. H.; Sheppard, E. W.; McCullen, S. B.; Higgins, J. B.; Schlenker, J. L. *J. Am. Chem. Soc.* **1992**, *114*, 10834.
(26) Zhao, X. S.; Lu, G. Q. M.; Millar, G. J. *Ind. Eng. Chem. Res.* **1996**, *35* (7), 2075.
(27) Sayari, A. *Chem. Mater.* **1996**, *8*, 1840.
(28) Ying, J. Y.; Mehnert, C. P.; Wong, M. S. *Angew. Chem. Int. Ed.* **1999**, *38* (1−2), 56.
(29) Carvalho, W. A.; Wallau, M.; Schuchardt, U. *J. Mol. Catal. A−Chem.* **1999**, *144* (1), 91.
(30) Franke, O.; Rathousky, J.; Schulz-Ekloff, G.; Starek, J.; Zukal, A. New mesoporous titano-silicate molecular sieve. In *Zeolites and Related Microporous Materials: State of the Art 1994;* Studies in Surface Science and Catalysis 84; Weitkamp, J., Karge, H. G., Pfeifer, H., Hölderich, W., Eds.; Elsevier Science: New York, 1994; p 77.
(31) http://www.bris.ac.uk/Depts/Chemistry/MOTM/mcm41/mcm41c.htm.
(32) Zhou, W. *Micron* **2000**, *31*, 605.

correction, the geometric distortions would be interpreted as large area phase shifts due to the object. This correction also largely eliminates the Fresnel fringes evoked by the biprism.

3. Results

To compare the results of conventional electron microscopy and electron holography, the polymer sample was stained with OsO_4. One recognizes typical lamellar structure of the sample. When darker regions are carefully looked into, individual grains of osmium become visible (Figure 10). In the hologram, the strong bending of the interference fringes shows the strong phase modulation produced by the sample; this is caused by the heavy metal osmium. In Figure 12, examples are shown of distorted hologram fringes of stained polyethylene.

In Figure 13a, one of the first reconstructed phase images of unstained styrene block butadiene copolymer is shown. On the top left, lamellae are visible, and in addition, fine fringes of the hologram are still present crossing from the left (below) to the right (top). The surface of the film shows strong waviness and kinks, i.e., the topography dominates the micrograph. This is due to the superb large-area-contrast properties of holography: also, unwanted larger area structures such as thickness variations, produced, e.g., by a microtome, show up in a height contrast.

What can we do to avoid these problems? We have to look for a smoother area of the sample. Doing so, we find results such as in Figure 13b. Both, lamellae and an onion structure situated at the middle of the phase image are present. Figure 14 also shows lamellar structures and an onion structure again. A phase profile drawn normal to the lamellae clearly suggests a lamellar long period of 45 nm. Additionally, at the *y*-axis, the phase difference of $1/36\pi$ between PS and PB lamellae can be read out. The contrast in the phase images is still poor; nevertheless, the inner structures of the polymer are clearly visible. The dose applied to record a hologram of the block copolymer amounted to about 500 e/pixel according to 18 e/Å^2. This value is in the range of the critical dose given for PS.[18,33]

As a second sample, we looked at the mesoporous silica MCM-41. The TEM image of the sample recorded in a conventional manner, namely, at strong defocus is given in Figure 15. The defocus is clearly visible at the edge of the sample giving rise to broad Fresnel fringes. In Scherzer focus, the porosities do not show any contrast. Consequently, one has to defocus up to 1.2−1.4 μm to image the hexagonal arrangement of the porosities; however, the hexagonal shape of the porosities cannot be recognized. Besides the hexagonal lattice, a lamellar phase appears in the middle of the micrograph. In Figure 16, the phase image reconstructed from a hologram is shown. Evidently, the regular hexagonal shape and ordering of the porosities resembling honeycombs is imaged. Again, the strong difference to conventional electron microscopy occurs at the edge of the sample. There are no more Fresnel diffraction fringes detectable; the edge of the specimen is clearly reproduced.

(33) Tsuji, M. Electron Microscopy. In *Comprehensive Polymer Science*; Sir Allen, G., Bevington, J. C., Eds.; Pergamon Press: Elmsford, NY, 1990; Vol. 1, p 806.

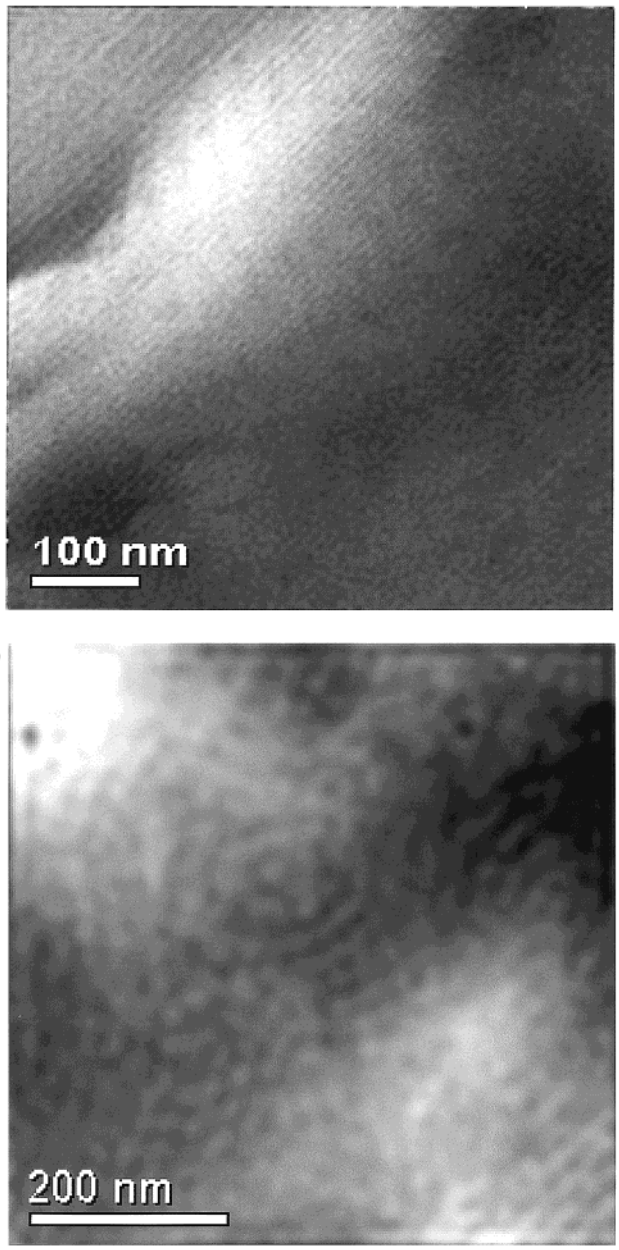

Figure 13. (a) Reconstructed electron phase images of unstained styrene/butadiene block copolymer. The surface of the film shows strong waviness and kinks, i.e., the topography dominates the micrograph. (b) Pearl-beadlike features appear in the electron phase image corresponding to the structural units of polystyrene lamellae.

To obtain micrographs of this quality, it is essential to process the phase images under numerical reconstruction. Mainly, the following three techniques were applied: with a phase wedge, it is possible to eliminate strong thickness differences in the sample; phase jumps greater than 2π can be removed ("phase unwrapping"), and the phases can be shifted by an offset.

4. Discussion and Résumé

It was shown that it is possible to image weak phase objects and beam sensitive materials by electron holography. The striking advantage of electron holography in contrast to conventional electron microscopy techniques is given by the preserved phase information. Neither staining nor defocus are needed to image weak

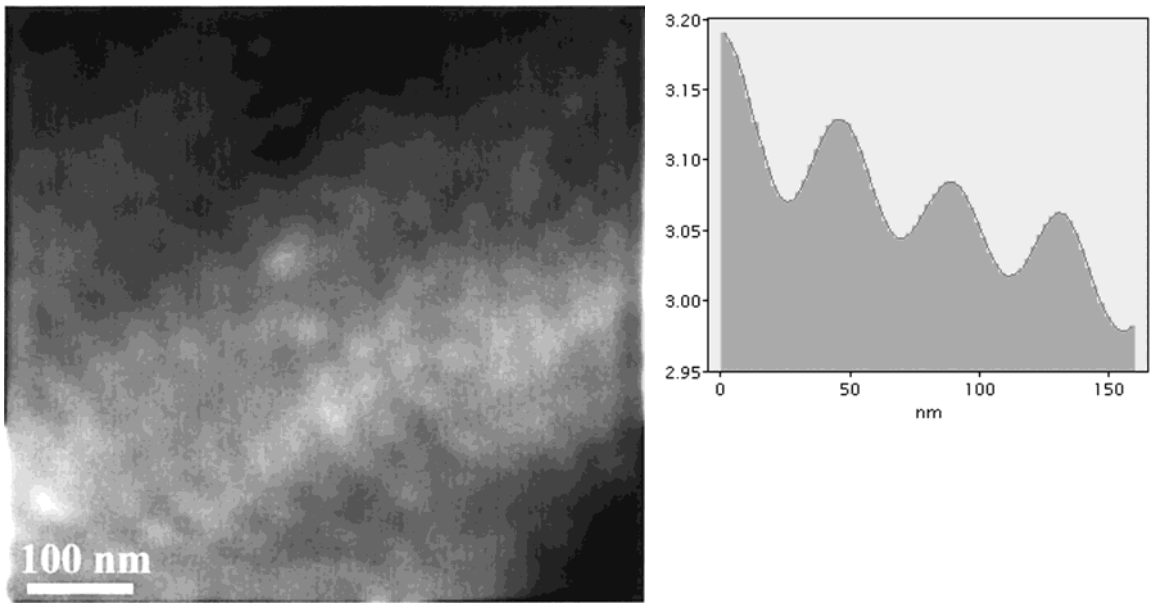

Figure 14. Reconstructed electron phase image of lamellar styrene/butadiene block copolymer with height profile indicating lamellar long period of 45 nm.

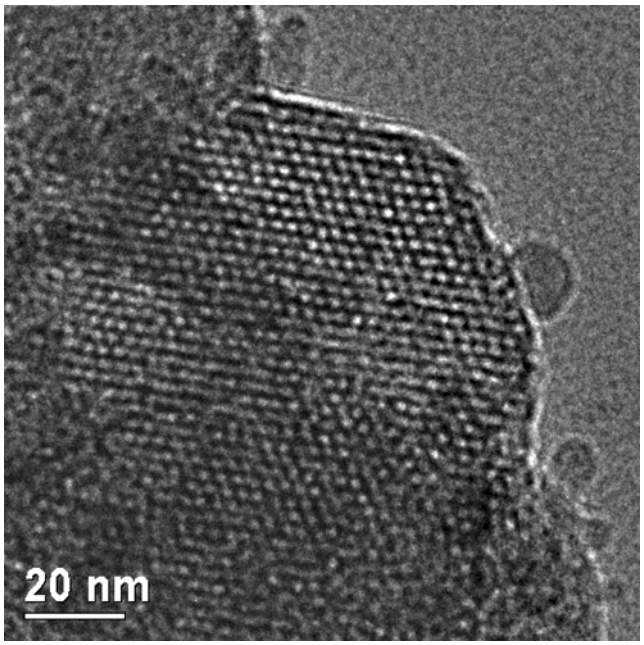

Figure 15. Conventional TEM micrograph of mesoporous silica MCM-41 at defocus of $\Delta f = -1.2$ μm.

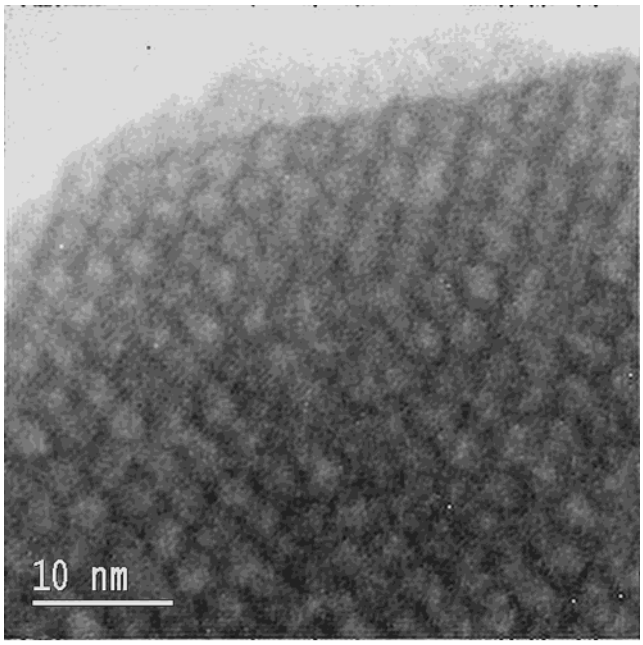

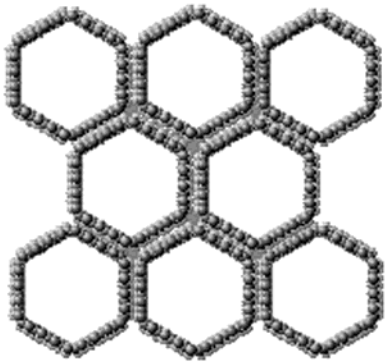

Figure 16. Reconstructed phase image of silica MCM-41 with idealized crystal lattice (below).

phase structures. In this way, artifacts can be avoided but not the limitations posed by beam sensitivity and inelastic scattering.

At first glance, the phase-separated structures of the block copolymer in Figure 13b (reconstructed phase image of electron hologram) appear quite different from that observed in its conventional TEM image (Figure 10). However, a closer inspection reveals that the pearl-beadlike features appearing in the phase image correspond to the structural units of PS lamellae. These beads and "gaps" (the regions of poorer contrast) may be arranged to form a PS lamella which results in the structure very similar to that observed with atomic force microscopy as illustrated in Figure 17. Since the contrast in the holographic image is strongly influenced by density variations across the sample, this observation would indicate that the PS lamellae are actually formed by PS chains of different lengths. The latter could be possible due to the highly asymmetric nature of copoly-

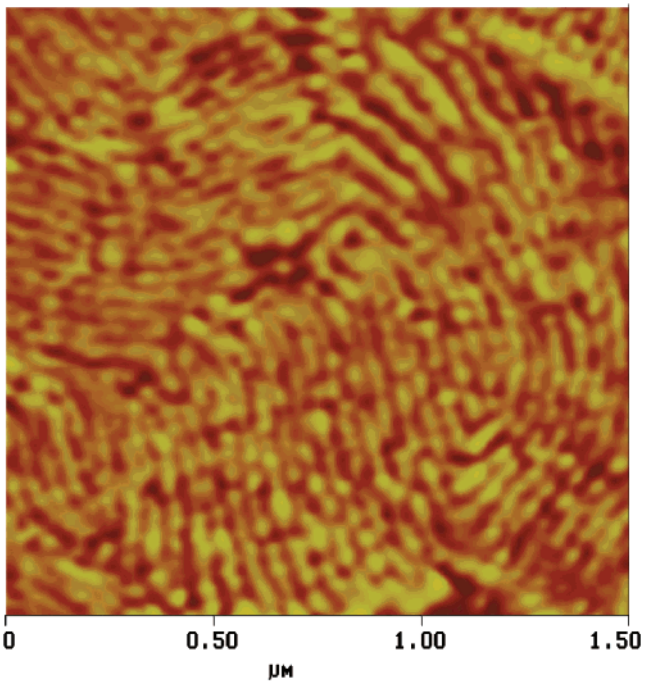

Figure 17. Tapping mode AFM phase image of the styrene/butadiene block copolymer: ultramicrotomed (−120 °C) face of bulk sample. Dark regions correspond to the soft butadiene phase.

mer molecules which consist of PS end blocks of different lengths. This is an indication of further potential of holography in achieving new information on the structures of polymeric materials.

The contrast of the phase micrographs of the polymer samples has to be improved. One measure could be to use smoother samples. Thin sections may be deformed during the cutting process. As a consequence, waviness, ripples, and microscopic roughness of the sample surface are produced. Subsequent smoothing of the thin section could bring about better results, because the phase shift caused by surface roughness will be minimized. Another approach is to use solution casting to prepare smooth films of optimum thickness.

For the silica, a resolution of about 4 Å is possible as indicated by the Fourier transform. Thus, at higher magnification, it should be possible to examine the fine structure of the porous walls. The hexagonal shape of the porosities is clearly visible, and the wall formation was imaged without the disturbing oscillations for higher frequencies of the phase transfer function.

Acknowledgment. The author sincerely acknowledges Mrs. Goerlitz in Halle for the preparation of thin sections of the block copolymer and Prof. Goldberg in Dresden for many helpful discussions. R.A. thanks the Kultusministerium des Landes Sachsen-Anhalt and the Max-Buchner-Forschungsstiftung for financial support. In addition, we thank the BASF-AG for kindly providing the block copolymer sample.

CM011140Q